Infrared Physics & Technology 115 (2021) 103723

Contents lists available at ScienceDirect

Infrared Physics and Technology

journal homepage: www.elsevier.com/locate/infrared

Regular article

Improving passivation properties using a nano-crystalline silicon oxide layer for high-efficiency TOPCon cells

Muhammad Quddamah Khokhar [a], Sanchari Chowdhury [a], Duy Phong Pham [b,c], Shahzada Qamar Hussain [d], Eun-Chel Cho [a,*], Junsin Yi [a,*]

[a] College of Information and Communication Engineering, Sungkyunkwan University, Suwon 16419, South Korea
[b] Division of Computational Physics, Institute for Computational Science, Ton Duc Thang University, Ho Chi Minh City, Viet Nam
[c] Faculty of Electrical and Electronics Engineering, Ton Duc Thang University, Ho Chi Minh City, Viet Nam
[d] Department of Physics, COMSATS University Islamabad, Lahore Campus, Lahore 54000, Pakistan

ARTICLE INFO

Keywords:
nc-SiO_x
Poly-Si
Passivation characteristics
TOPCon solar cells
High efficiency

ABSTRACT

High conversion efficiency can achieve by superior surface passivation and material quality. In this study, a novel passivation contact structure based on nanocrystalline silicon oxide (nc-SiO_x) films was investigated. Traditionally, poly silicon junctions in tunnel oxide passivated contact (TOPCon) solar cells possess exceptional junction characteristics, but current losses are noted due to their optical absorption if they are applied in solar cell devices. In this study, we replaced the poly-Si layer in TOPCon solar cells with nc-SiO_x to enhance transparency. By employing the nc-SiO_x layer, effective surface passivation, carrier selectivity, electrical properties and optical transmission can be used to improve, all are vitally important in devise operation. We optimized the deposited nc-SiO_x layer on an ultra-thin (~1.5 nm) silicon dioxide (SiO_2) tunnel oxide layer to improve recombination current density and carrier lifetime. The passivation characteristics were improved by varying the annealing temperature and thickness of the nc-SiO_x layer. The 50 nm thick nc-SiO_x layer was capable of yielding a high implied open-circuit voltage (i-V_{oc}) of 739 mV and low contact resistivity (ρ) of 14.2 (mΩ/cm^2) in addition to a low depleted recombination current density (J_o) of 1.1 fA/cm^2 with a post-deposition annealing temperature up to 950 °C. Improved passivation characteristics are the result of a more prominent annealing temperature. Our proposed technique has immense potential for achieving higher efficiency for fabricating various structures of TOPCon solar cells. As per AFORST Het simulation results by using nc-SiO_x for TOPCon structure, we got V_{oc} of 761.5 mV, J_{sc} of 43.5 mA/cm^2, FF of 83%, and η of 27.49%, respectively.

1. Introduction

Currently, photovoltaic energy production is considered the subject of significant research attention owing to its environmentally friendly, globally consented, and renewable characteristics. Crystalline silicon (c-Si) is commonly used to fabricate solar cells because of its abundance in nature, low cost, and excellent performance. Presently, above 95% of overall photovoltaic production is shared by c-Si solar [1]. To further enhance the conversion efficiency of c-Si solar cells, the minority charge-carrier recombination losses at the interfaces between the Si absorber and electrodes must be reduced while maintaining efficient majority charge-carrier extraction [2–4]. Recently, various passivating contact technologies, such as polycrystalline Si on oxide (POLO), and poly-Si-based passivating contacts on thin oxides and tunnel oxide passivated contacts (TOPCon) have demonstrated excellent passivation and carrier selectivity characteristics [5–10]. Thin buffer layers of SiO_x capped with doped poly-Si or semi-insulating poly-Si (SIPOS) approaches were first investigated during the 1980s [11–13]. Better passivation performance was observed with an approach using SIPOS alloyed with oxygen compared to pure poly-Si layers, but the produced thin films were too resistive for current extraction from solar cells [12–14]. Recently, enhanced solar cell characteristics have been reported using similar approaches on the rear side for two-sided contact solar cells and interdigitated back contact (IBC) devices without oxygen alloying [15–21]. With exceptional passivating junction characteristics for the front side contact solar cell, the rear side contacting scheme is the factor limiting efficiency. To outspread the application of passivating contacts for the rear side, additional requirements must be met. To overcome parasitic

* Corresponding authors at: 2066, Seobu-ro, Jangan-gu, Suwon 16419, Gyeonggi-Do, South Korea.
E-mail addresses: quddamah@skku.edu (M.Q. Khokhar), phamduyphong@tdtu.edu.vn (D.P. Pham), echo0211@skku.edu (E.-C. Cho), junsin@skku.edu (J. Yi).

https://doi.org/10.1016/j.infrared.2021.103723
Received 15 December 2020; Received in revised form 9 March 2021; Accepted 19 March 2021
Available online 24 March 2021

absorption losses, rear-side films must be highly transparent, while providing excellent transport and superior passivation for the selected charge carrier. To minimize absorption loss, we report a novel rear side-area passivating electron contact that improves the transparency by replacing a part of the doped poly-Si layer. The novel contact structure includes a thin thermally grown SiO_2 layer on the c-Si wafer surface capped by a phosphorus-doped nanocrystalline silicon oxide (nc-SiO_x). The plasma-enhanced chemical vapor deposition (PECVD) system of (SNTEK company) with a frequency of 13.56 MHz, was used for the growth of the nc-SiO_x layer. The PECVD process has the advantage that it allows single-sided deposition instead of the wrap-around deposition observed during the low-pressure chemical vapor deposition process [22]. Moreover, the temperature stability of passivation is improved owing to the presence of a thermally grown SiO_2 layer, resulting in a broad thermal processing window.

A wide bandgap material, nc-SiO_x, was introduced to reduce optical absorption. The optical and electrical characteristics could be varied by changing the oxygen content. The conductive properties of the n-doped nc-SiO_x were found at low oxygen concentrations with phosphorus doping. The annealing process is an important process for activating the dopant and developing films required for emitter contact. During the annealing process, the surface morphology varied throughout. The Si precipitates into small grains of nano-Si, while the O_2 acts as insulation and forms SiO_2 on the grain boundaries [23]. The consequences of O_2 assimilation are the result of a reduction in grain growth. For higher O_2 concentrations, Carrier transport is resulted by tunneling via thin SiO_x shells for higher O_2 concentrations [24].

The junction properties were analyzed by varying the thickness and annealing time of the deposited layer. Hydrogen passivation in forming gas annealing (FGA) was investigated after the influence of each parameter. Additionally, our research focused on the experimental designs to explain the physical mechanisms accountable for melioration and optimization of the passivation characteristics of symmetric structures using a Quasi-Steady-State Photoconductance (QSSPC) measurement system.

2. Experimental

Czochralski-grown phosphorus-doped n-type wafers (200 μm thick with 3–5 Ω-cm,) were used in this study. The first step was the removal of surface defects by employing an etching solution comprising sodium hydroxide (NaOH) at 70–80 °C for approximately 10 min. Further, samples were consecutively cleaned by employing the standard RCA-1 and RCA-2 cleaning processes to remove organic and metallic impurities [25]. Afterward, the samples were dipped in HCl solution and then in HF solution for 2 min each. Finally, the deionized water was used for the cleaning of samples. The cleaned samples were immediately placed in a thermal oxide furnace. The thermally growth of a SiO_2 tunnel layer with a thickness of approximately 1.5 nm on the front and back sides of the cleaned Si wafer was conducted in a furnace. The SiO_2 layer was grown by thermal oxidation of the cleaned silicon wafer at a temperature of 600 °C with an O_2 flow rate of 10 L/min for 30 min. Finally, the samples were detached from the thermal furnace for the deposition of nc-SiO_x. The deposition was performed using PECVD in the presence of SiH_4, H_2, CO_2, and PH_3 gases at a temperature of approximately 110 °C, and thicknesses of 30, 40, and 50 nm were obtained. For deposition of nc-SiO_x, we used 1.5 T pressure and 35 mW/cm^2 power, respectively. Optimized PECVD deposition conditions of phosphorus-doped nc-SiO_x material were reported in our previous paper [26]. Electrical and optical properties of n-type nc-SiO_x were optimized by introducing SiH_4, H_2, CO_2, and PH_3 at ratios of 4, 500, 2, and 0.08, respectively [26]. All samples synthesized in this study were exposed to post-deposition annealing (PDA) at 850, 900, 950, or 1000 °C for more crystallization. Finally, FGA was performed for 2 h at 400 °C. The parameters used to obtain passivated nc-SiO_x contacts are listed in Table 1. The procedure is described in detail below.

Table 1
Parameters and results of symmetric structure for SiO_x/nc-SiO_x passivated contacts after FGA.

Sample	Annealing Temp. (°C)	FGA (°C)	Thickness (nm)	Lifetime (μs)	J_O (fA/cm^2)	i-V_{oc} (mV)
1	1000	400	30	1466	2.92	717
2	1000		40	2035	1.51	730
3	1000		50	2397	1.35	736
4	950		30	1919	1.86	726
5	950		40	2530	1.1	731
6	950		50	2918	1.1	739
7	900		30	1013	3.97	709
8	900		40	1547	1.93	729
9	900		50	1877	1.6	733
10	850		30	1096	5.15	705
11	850		40	1118	3.85	711
12	850		50	611	8.17	698

The symmetric structures synthesized through these two approaches are shown in Fig. 1. The ultrathin SiO_2 tunnel oxide layer and nc-SiO_x layer with various thicknesses were confirmed through high-resolution transmission electron microscopy (HRTEM) and spectroscopic ellipsometry (VASE, JA Woollam). The passivation characteristics were evaluated using a QSSPC measurement system (WCT Sintron, 120). The transfer length method (TLM) was used to obtain the contact resistivity (ρ_c). We used the TLM method by etching the polysilicon to measure the contact resistivity. To investigate the current pathway, the region between the TLM pads was repetitively etched in $SF_6/O_2/Ar$ plasma using the aluminum pads as an etching mask, and the samples were measured after each etch process by TLM. The plasma-enhanced chemical vapor deposition (PECVD) system of (SNTEK company) with a frequency of 13.56 MHz and thermal furnace of EM TECH company are used during the experiment. Structural characteristics were evaluated by Raman spectroscopy (Ramboss 500i, Dongwoo Optron Co., Ltd.). X-ray photoelectron spectroscopy (XPS) experiments were carried out on a Physical Electronics PHI5000 Versa Probe II photoelectron spectrometer with a mono-chromated Al-Ka source operated in a high-power mode at 100 W. To increase the probing depth, the takeoff angle was set to 85. The Si2p peak was measured with a pass energy of 5.85 eV and 25 meV/step.

3. Results and discussion

3.1. Observation of structure characteristic and passivation characteristics at various thicknesses of nc-SiO_x on different annealing temperature

The HRTEM image of the ultrathin SiO_2 layer capped with the nc-SiO_x layer observed at a scale of 1 nm is shown in Fig. 2. The thickness of this layer was recorded as 1.5 nm. The SiO_2 layer with a thickness greater than 1.6 nm has previously been reported to exhibit poor passivation properties due to the reduced degree of dopant diffusion from nc-SiO_x to the c-Si wafer owing to the thicker SiO_2 layer [27]. The structural analyses of such nc-SiO_x layers using Raman spectroscopy are shown in Fig. 3a and b. Crystalline volume factor (X_c) as shown in Fig. 3c was derived from the data using the relation $X_c = I_{518,519}/(I_{518,519} + I_{480})$, in which $I_{518,\ 519}$ and I_{480} are the integrated areas extracted from Gaussian fitting at 518, 519 and 480 cm^{-1}, respectively. We can see in Fig. 3a that the nc-SiO_x layer structure before annealing appears to present a mix phase of crystalline and amorphous, which is characterized by a Raman peak at 480 cm^{-1} and 518 cm^{-1}, mainly visible at thicknesses above the value of 50 nm thick. On the contrary, for thicknesses in the range of 30–50 nm, the structure can be regarded essentially as an amorphous phase, as defined by a broad spectral range centered around 480 cm^{-1}. It has been known that the growth of crystalline phase in silicon films during plasma deposition is generally initiated through a first incubation amorphous phase followed by

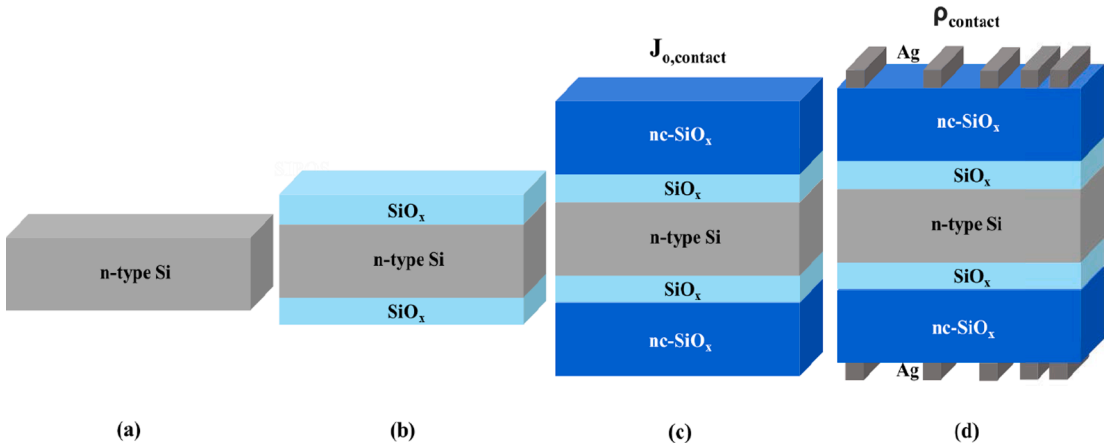

Fig. 1. Schematic diagrams of nc-SiO_x passivation: (a) wafer characteristics, (b) passivation characteristics of the SiO_x tunnel layer (τ_{eff}, iV_{oc}, J_o, and thickness), (c) passivation properties (τ_{eff}, iV_{oc}, J_o, and thickness) and recombination current density (J_o) of SiO_x/nc-SiO_x passivated contact, and (d) effective contact resistivity (ρ) of SiO_x/nc-SiO_x passivated contacts.

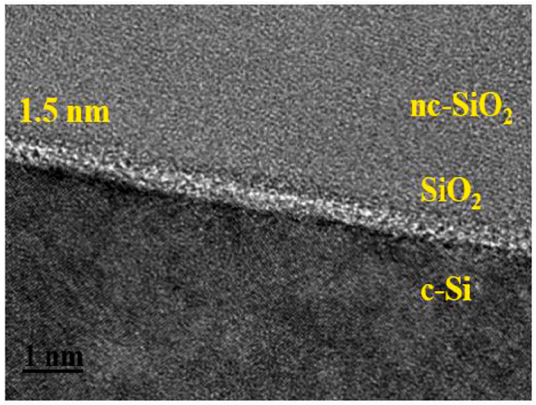

Fig. 2. HRTEM images of ultrathin (~1.5 nm) SiO_2 layer.

nucleation and, finally, crystalline phase formation [27–29]. In this process, nucleation-growth aggregation plays an important role to prompt subsequent crystalline particles. As shown in Fig. 3b, raman spectra showing a clear tendency towards lower amorphous fraction with increasing temperature. As shown in Fig. 3b, the crystalline phase of n-nc-SiO_x layer can be initiated and more prominent at all thickness of 30, 40, and 50 nm after annealing at 950 °C in thermal furnace. We done Raman spectroscopy only at 950 °C because we got ameliorated passivation properties at 950 °C. Already in the as-deposited state, the Raman spectrum is dominated by the transverse optical (TO) c-Si phonon with a peak around 518 cm^{-1}. However, the signal still shows a pronounced shoulder at wavenumbers between 400 cm^{-1} and 510 cm^{-1}, which can be attributed to amorphous Si. After 1-hour higher annealing temperature at 950 °C, the amorphous fraction is decreasing further and lateral inhomogeneities vanish (not shown here). The amorphous contribution almost disappears for a dwell temperature of 950 °C, meaning that the layer is almost fully crystalline. The annealing temperature plays significant role in prompting the rapid growth of crystalline phase in the nc-SiO_x layer even with a low or higher thickness. Based on the nucleation kinetics, the crystalline phase may grow rapidly and increase in thickness. This is observable in Fig. 3c where the value of X_c increases with thickness of nc-SiO_x layer as well as increases with annealing temperature. Examination of the chemical state of the silicon by XPS depicted an oxidation induced splitting of the Si2p peak as described in Fig. 4. Investigation of the oxidation states was executed by deconvolution of the silicon 2p peak. It is known as a rule of thumb that the peak shifts 1 eV per oxidation state. The exact parameters were taken from Ref. 37 (Si^{1+}: 0.9 eV, Si^{2+}: 1.7 eV, Si^{3+}: 2.7 eV, Si^{4+}: 3.7 eV). The deconvolution of the peak revealed the presence of silicon suboxides in the material. The observed evolution of the Si^{n+} distribution with 50 nm thick layer of nc-SiO_x, despite the fixed oxygen content in the present study, indicates a phase separation. Deviation in the passivation characteristics of samples deposited by nc-SiO_x were analyzed. The passivation properties at thicknesses of 30, 40, and 50 nm were equated. Then, the nc-SiO_x deposited samples were annealed at various temperatures in the range of 850–1000 °C. The results of the PDA clarified the breaking of the silicon-hydrogen bond as well as accompanying hydrogen diffusion within the c-Si substrate and phosphorous diffusion via the tunnel oxide layer within the n-type substrate. As mentioned earlier, the passivation quality was enhanced by the insertion of the tunnel oxide layer. In this study, passivation of the tunnel oxide junction structure was observed to be excellent for the sample subjected to 950 °C thermal annealing. However, the passivation quality decreased with heat treatment above 950 °C, which means at 1000 °C. This is reportedly attributed to the local disruption of the tunnel oxide layer. This disruption is not easy to observe through TEM and XPS measurements due to the fine area analysis on the atomic scale. A bifacial structure such as used for the QSSPC measurement was employed. Substantial improvements in passivation characteristics were observed after PDA when the nc-SiO_x layer thickness was approximately 50 nm at 950 °C. As the nc-SiO_x layer thickness approached 50 nm, considerable improvements were detected in both lifetime (τ_{eff}) and i-V_{OC}. Fig. 5(a) depicts the τ_{eff} and i-V_{OC} of the deposited samples from the evaluated thicknesses as a function of the post-deposition annealing temperature (T_{PDA}). Both τ_{eff} and i-V_{OC} of the deposited annealed samples were found to be more prominent as compared to the as-deposited sample. The results of τ_{eff} and i-V_{OC} improved at all examined thicknesses as the annealing temperature increased to 950 °C, after which they diminished for higher annealing temperature around 1000 °C. Fig. 5(b) demonstrates the J_o of the three different nc-SiO_x thickness samples in response to the T_{PDA}. J_o diminished with an increase in annealing temperature up to 950 °C and then J_o starts to increase as the annealing temperature increased further up to 1000 °C. Particularly high increases in τ_{eff} and i-V_{OC} as well as reductions in J_o compared to the as-deposited state of the nc-SiO_x layer, at the annealing temperature of approximately 950 °C, were ascribed to the ameliorated chemical passivation of ultrathin SiO_2 due to the decreased field-effect passivation owing to carrier selectivity [28]. The best passivation characteristics were observed for the deposited sample with the 50 nm thick nc-SiO_x layer after the PDA at 950 °C, with the highest lifetime and i-V_{OC} of ~2446 μs and ~728 mV, respectively, and lowest J_o of 1.33 fA/cm^2.

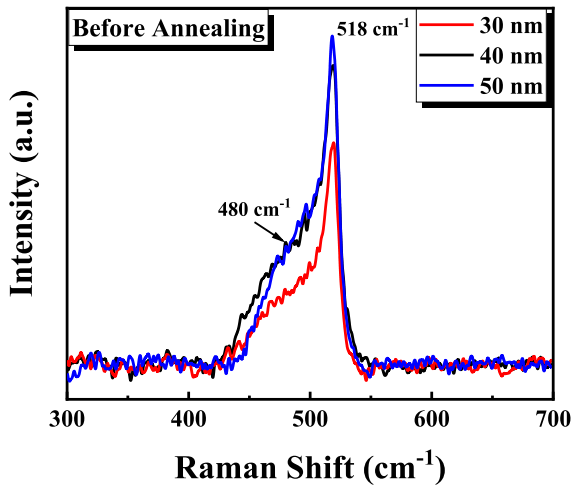

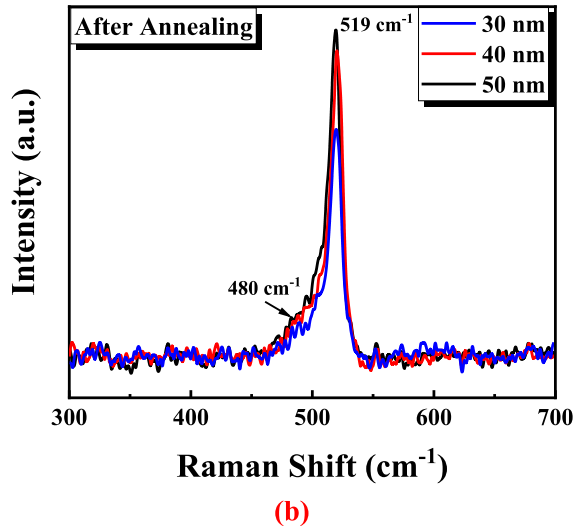

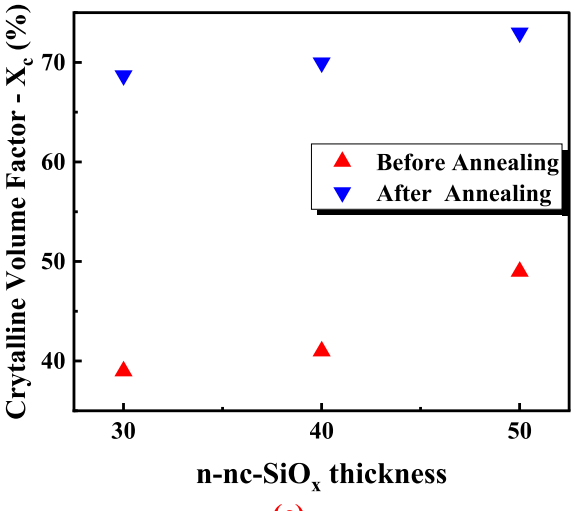

Fig. 3. Raman spectra of n-nc-SiO_x layers: a) Before and b) after annealing at 950 °C; and c) the crystalline volume factors (X_c) of n-nc-SiO_x layers before and after annealing at 950 °C as a function of thickness.

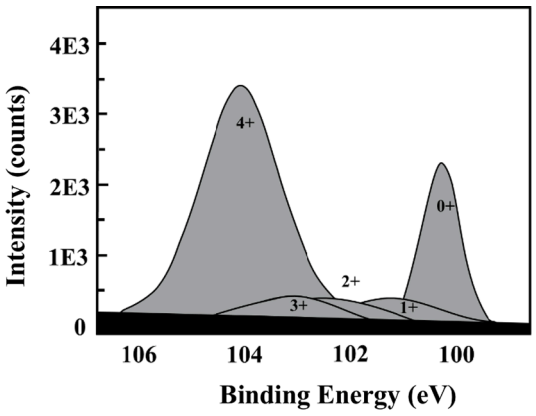

Fig. 4. XPS spectra of Si 2p peak photo-electron spectrum of a nc-SiO_x layer deposited.

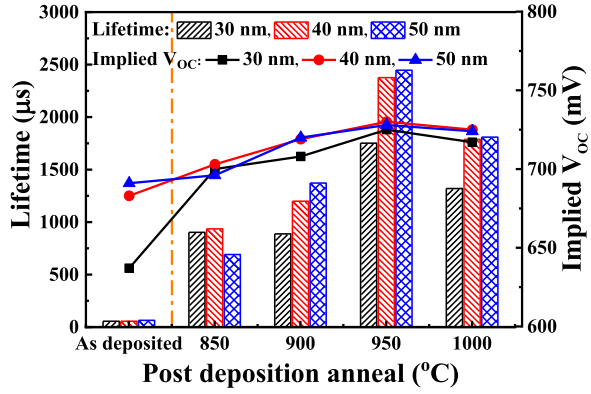

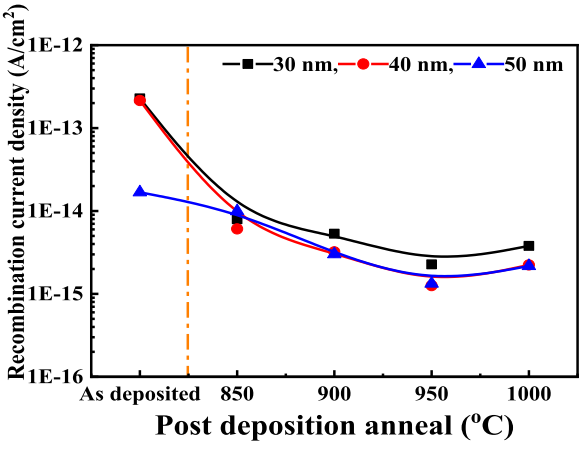

Fig. 5. (a). Minority carrier lifetime and implied open-circuit voltage as functions of T_{PDA} for three nc-SiO_x layer thicknesses at injection level 1×10^{15}. (b). Recombination current density as a function of T_{PDA} depending on nc-SiO_x layer thickness.

3.2. Improvement in passivation after FGA treatment

The passivation characteristics of symmetric structure enhanced further when FGA was performed at 400 °C for 2 h via rapid thermal processing on three different thicknesses of 30, 40, and 50 nm nc-SiO_x layer which were already exposed to post-deposition annealing (PDA) at 850, 900, 950 °C or 1000 °C. The highest lifetime and the i-V_{OC} were achieved up to 2.918 ms and of 739 mV on 50 nm thick nc-SiO_x layer

which exposed to post-deposition annealing (PDA) at 950 °C, when FGA treatment was performed for nc-SiO_x layers with thicknesses of 30–50 nm. The measured lifetime and the i-V_{OC} were extracted at the injection level ($1.0E^{+15}$ cm^{-3}). in that case, our value highest passivation value of lifetime comes around 2.918 ms and of 739 mV at 50 nm, as shown in lifetime spectrum diagram Fig. 6(c). A substantial reduction in J_o to 1.1 fA/cm^2 was observed at the 50 nm thick nc-SiO_x layer which exposed to post-deposition annealing (PDA) at 950 °C and then J_o starts to increase as the annealing temperature increased further up to 1000 °C. In this study, passivation of the tunnel oxide junction structure was observed to be excellent for the sample subjected to 950 °C thermal annealing. However, the passivation quality decreased with heat treatment above 950 °C, which means at 1000 °C. FGA treatment induced a substantial decrease in interface defect density (D_{it}), which enhanced passivation. The highest lifetime and the i-V_{OC} were achieved due to the hydrogen passivation process means after FGA. It is thought that dangling silicon bonds in the interface and tunnel oxide layer were passivated by hydrogen. To improve the passivation quality of the tunnel oxide layer, it is important to control the properties and stoichiometry of the tunnel oxide layer. The FGA treatment on the phosphorus-doped nc-SiO_x layer increased hydrogen activation on both sides of the nc-SiO_x layer as well as of the tunnel oxide interface. This treatment permitted the best passivation at 50 nm thick phosphorus-doped nc-SiO_x layer. FGA led to a minimal J_o value, showing that this structure would produce a higher-efficiency TOPCon cell. Fig. 6(a) shows improvements in τ_{eff} and i-V_{OC} following FGA treatment for deposited samples at different thicknesses. Both τ_{eff} and i-V_{OC} values increased at higher nc-SiO_x layer thicknesses and higher T_{PDA} values. Fig. 6(b) depicts the change in J_o after FGA at similar conditions as above. J_o was found to be as little as ~1.1 fA/cm^2 after FGA. We used the minority-carrier lifetime measurement as initially rough parameters to estimate the passivation quality of the resulting wafer surface. Fig. 6(c) shows the effective minority carrier lifetime data of the initial passivated wafer with various thicknesses of the nc-SiO_x layer which exposed to post-deposition annealing (PDA) at 950 °C.

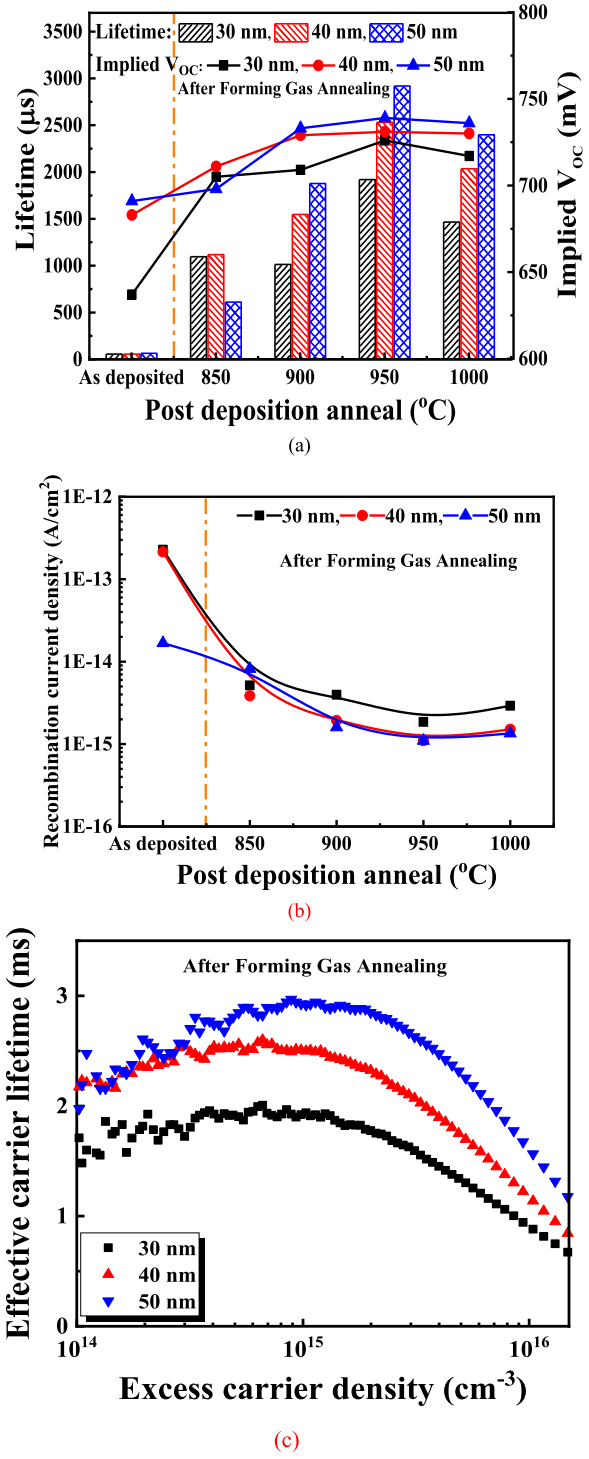

Fig. 6. (a). Improvement in minority carrier lifetime and implied open-circuit voltage as a function of T_{PDA} and nc-SiO_x layer thickness after FGA at injection level 1×10^{15}. (b). Improvement in rear recombination current density as a function of T_{PDA} and nc-SiO_x layer thickness after FGA. (c) Effective minority carrier lifetime data of various thickness at 950 °C.

3.3. Analysis of SiO_x/nc-SiO_x contact passivation properties (J_o and ρ) and (D_{it} and i-V_{oc})

To examine the passivated contact characteristics at the minimum J_o value, we first identified low $\rho_{contact}$ values, which permit selective carrier transport by a particular SiO_x tunnel layer. To analyze the impact of the leading SiO_x/nc-SiO_x passivated contacts, nc-SiO_x layers were deposited on both sides of the SiO_x layers, and thereafter, FGA was performed. The J_o values were extracted using QSSPC for the SiO_x/nc-SiO_x contacts. After the FGA on SiO_x/nc-SiO_x, a considerable enhancement of the overall quality was achieved. Thermal annealing at 950 °C and FGA at 400 °C resulted in the lowest values of J_o and ρ, but at 1000 °C thermal annealing and FGA at 400 °C resulted in the lowest values of ρ and the highest value of J_o. The results presented in Fig. 7(a) demonstrate that the total contact resistance declined gradually with increasing annealing temperature, whereas the drop was precipitous for the sample annealed around 1000 °C. Thus, this is considered indirect evidence of local disruption of the tunnel oxide layer. Based on the total resistance, the resistivity of the tunnel oxide layer was deducted to separate the layers of the sample structure by considering the thickness and sheet resistance measurements of the nc-SiOx layer and the substrate properties. The improvement in J_o the value for the 50 nm SiO_x/nc-SiO_x passivated contact annealed at 950 °C was more prominent compared to samples annealed at 850 °C and 900 °C. Passivated contact with FGA samples ensued in diminished values (1.1 $fAcm^{-2}$) at 50 nm, showing limited surface recombination as well as improved passivation compared to annealing at 850 °C (8.17 $fAcm^{-2}$) and 900 °C (1.6 $fAcm^{-2}$).

For SiO_x/nc-SiO_x passivated contact FGA, an improvement was seen at 400 °C, yielding the lowest J_o and ρ values. As J_o and ρ values decreased, tunneling efficiency increased. Fig. 7(a) shows J_o and ρ of the deposited samples with various nc-SiO_x thicknesses as a function of T_{PDA}. For all thicknesses, J_o and ρ values declined as annealing temperature increased up to 950 °C. Fig. 7(b) depicts the comparison of both J_o and ρ results with those of other research groups worldwide. Comparing our results with those of other research groups such as Josua et al. [30] reveals that we achieved improved passivation results. In both

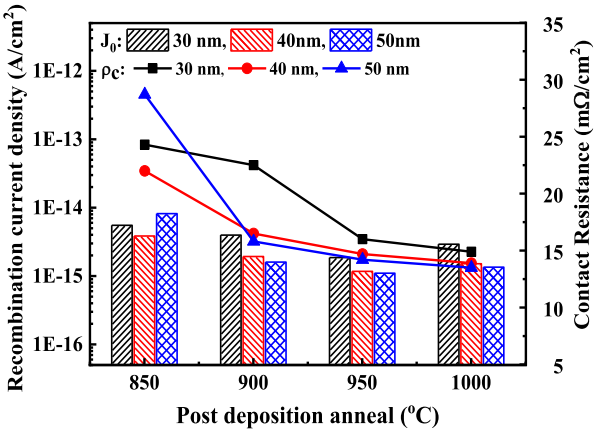

(a)

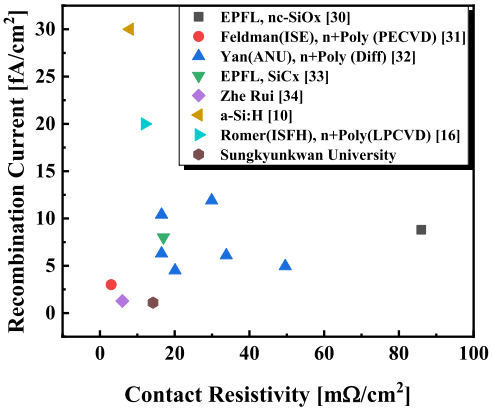

(b)

Fig. 7. (a). Improvements in recombination current density and contact resistance at various T_{PDA} and nc-SiO_x layer thickness after FGA. (b) Comparison between recombination current density and contact resistance from different studies.

studies, the main aim was to improve TOPCon solar cell efficiency using nc-SiO_x. However, the difference lies in the SiO_x growth method and thickness as well as deposition temperatures. The novelty of our results arose from different fabrication methods and treatment steps. Josua et al. used a chemical process for oxidation and a thin nc-SiO_x layer, thus requiring different annealing times and temperatures. In this study, we optimized the thickness of evaluated layers, N_2 atmosphere annealing, and FGA temperature and time.

To evaluate the passivation contact properties, maximum i-V_{oc} values and low interface trap density (D_{it}) were examined as they permit selective carrier transport by a particular SiO_x tunnel layer. The D_{it} of the tunnel oxide layer was quantitatively assessed by C-V measurement. The D_{it} was studied to evaluate the effect of SiO_x and nc-SiO_x quality on surface passivation. D_{it} is evaluated at the interface of SiO_x/nc-SiO_x; the lower the D_{it} value, the higher the i-V_{oc}. Fig. 8 confirms a decrease of the D_{it} due to the Si-O bonding transition induced by post-annealing. Further, the D_{it} of about 1.23×10^9 cm^{-2}/eV was achieved due to the H passivation process means FGA treatment. It is thought that dangling silicon bonds in the interface and tunnel oxide layer were passivated by hydrogen. To improve the passivation quality of the tunnel oxide layer, it is important to control the properties and stoichiometry of the tunnel oxide layer. An i-V_{oc} of 739 mV was achieved when the D_{it} was 1.23×10^9 cm^{-2}/eV, as shown in Fig. 8. However, the i-V_{oc} fell to 698 mV when D_{it} increased to 2.26×10^9 cm^{-2}/eV, after which i-V_{oc} continued to decrease. Reduction in D_{it} reduces the probability of carrier recombination which in turn influences the i-V_{oc} to improve. Thermal annealing

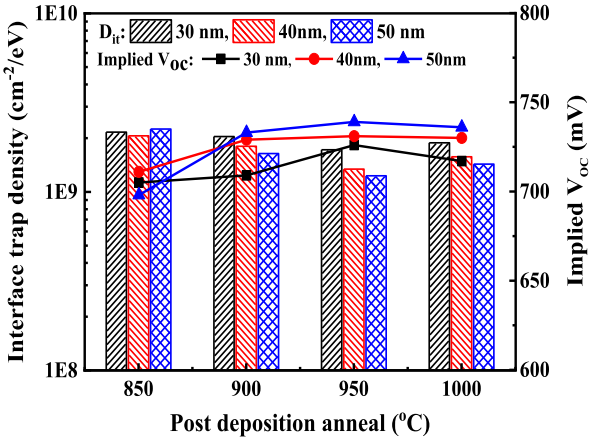

Fig. 8. Effect of D_{it} on i-V_{oc} as a function of T_{PDA} and nc-SiO_x layer thickness.

at 1000 °C and FGA at 400 °C of 50 nm thick nc-SiO_x films resulted in the lowest i-V_{oc} and highest D_{it}. But the thermal annealing at 950 °C and FGA at 400 °C of 50 nm thick nc-SiO_x films resulted in the highest i-V_{oc} and lowest D_{it}. For D_{it}, the decrease in i-V_{oc} owing to leakage became noticeable as the temperature rose. Therefore, the temperature characteristics of the contact solar cell are more sensitive to D_{it} [10,16,29–34].

4. Conclusion

This study aimed to improve passivation by employing an amended nc-SiO_x layer to enhance the implementation of nc-SiO_x for back surface films in high-performance TOPCon solar cells. We achieved improved passivation properties by applying a nc-SiO_x layer relatively thinner than that described in the current study. The improved thickness of the nc-SiO_x layer synthesized by PECVD was 50 nm at T_{PDA} with annealing at 950 °C and FGA at 400 °C. The Si–H bonds are broken by the PDA process that resulted in H diffusion into the c-Si substrate as well as reconstitution of the ultrathin SiO_x tunnel oxide layer owing to the establishment of pinholes. The most beneficial passivation properties were found after FGA because this process directly relinquished H into both the nc-SiO_x layer as well as the tunnel oxide layer. This research provides in-depth knowledge for future studies on the improvement of nc-SiO_x layers, which can assist the fabrication of TOPCon solar cells. nc-SiO_x with a thickness of 50 nm exhibited lower sheet resistivity as well as beneficial metal contact. Moreover, the T_{PDA} was diminished to mitigate high-temperature damage and achieve reduced costs. As per AFORST Het simulation results by using nc-SiO_x for TOPCon structure, we got V_{oc} of 761.5 mV, J_{sc} of 43.5 mA/cm^2, FF of 83% and η of 27.49%, respectively.

Declaration of Competing Interest

The authors declare that they have no known competing financial interests or personal relationships that could have appeared to influence the work reported in this paper.

Acknowledgment

This research was supported by grants from the New & Renewable Energy Technology Development Program of the Korea Institute of Energy Technology Evaluation and Planning (KETEP) grant funded by the Korean Ministry of Trade, Industry and Energy (MOTIE) (No. 20203030010310) and (No. 20203040010320).

References

[1] G. Masson, I. Kaizuka, IEA PVPS report-Trends in Photovoltaic Applications 2019, IEA, Paris, 2019.

[2] D. Rached, W.L. Rahal, Investigation of the interface defect density at pm-Si: H/c-Si and the surface recombination speeds on silicon heterojunction solar cells, Optik 223 (2020) 165575, https://doi.org/10.1016/j.ijleo.2020.165575.

[3] C. Battaglia, A. Cuevas, S. De Wolf, High-efficiency crystalline silicon solar cells: status and perspectives, Energy Environ. Sci. 9 (5) (2016) 1552–1576.

[4] U. Wurfel, A. Cuevas, P. Wurfel, Charge carrier separation in solar cells, IEEE J. Photovolt. 5 (1) (2015) 461–469.

[5] F.A. Lindholm, A. Neugroschel, M. Arienzo, P.A. Iles, Heavily doped polysilicon-contact solar cells, IEEE Electron Device Lett. 6 (7) (1985) 363–365.

[6] F. Feldmann, M. Bivour, C. Reichel, M. Hermle, S.W. Glunz, Passivated rear contacts for high-efficiency n-type Si solar cells providing high interface passivation quality and excellent transport characteristics, Sol. Energy Mater. Sol. Cells 120 (2014) 270–274.

[7] F. Feldmann, M. Simon, M. Bivour, C. Reichel, M. Hermle, S.W. Glunz, Carrier-selective contacts for Si solar cells, Appl. Phys. Lett. 104 (18) (2014) 181105, https://doi.org/10.1063/1.4875904.

[8] C. Hollemann, F. Haase, M. Rienäcker, V. Barnscheidt, J. Krügener, N. Folchert, R. Brendel, S. Richter, S. Großer, E. Sauter, J. Hübner, M. Oestreich, R. Peibst, Separating the two polarities of the poLo contacts of an 26.1%-efficient IBC solar cell, Sci. Rep. 10 (1) (2020), https://doi.org/10.1038/s41598-019-57310-0.

[9] F. Haase, S. Schafer, C. Klamt, F. Kiefer, J. Krugener, R. Brendel, R. Peibst, Perimeter recombination in 25%-efficient IBC solar cells with passivating POLO contacts for both polarities, IEEE J. Photovolt. 8 (1) (2018) 23–29.

[10] D.i. Yan, A. Cuevas, Y. Wan, J. Bullock, Passivating contacts for silicon solar cells based on boron-diffused recrystallized amorphous silicon and thin dielectric interlayers, Sol. Energy Mater. Sol. Cells 152 (2016) 73–79.

[11] Y.H. Kwark, R. Sinton, R.M. Swanson, SIPOS heterojunction contacts to silicon, in: 1984 International Electron Devices Meeting, IEEE, 1984, pp. 742–745.

[12] E. Yablonovitch, T. Gmitter, R. Swanson, Y. Kwark, A 720 mV open circuit voltage SiO x: c-Si: SiO x double heterostructure solar cell, Appl. Phys. Lett. 47 (1985) 1211–1213.

[13] J.-Y. Gan, R. Swanson, Polysilicon emitters for silicon concentrator solar cells, in: IEEE Conference on Photovoltaic Specialists, IEEE, 1990, pp. 245–250.

[14] T. Matsushita, H. Hayashi, N. Oh-Uchi, H. Yamoto, A SIPOS-Si heterojunction transistor, Jpn. J. Appl. Phys. 20 (1981) 75.

[15] F. Feldmann, C. Reichel, R. Müller, M. Hermle, Si solar cells with top/rear poly-Si contacts, in: 2016 IEEE 43rd Photovoltaic Specialists Conference (PVSC), IEEE, 2016, pp. 2421–2424.

[16] U. Römer, R. Peibst, T. Ohrdes, B. Lim, J. Krügener, E. Bugiel, T. Wietler, R. Brendel, Recombination behavior and contact resistance of n+ and p+ poly-crystalline Si/mono-crystalline Si junctions, Sol. Energy Mater. Sol. Cells 131 (2014) 85–91.

[17] Y. Tao, E.L. Chang, A. Upadhyaya, B. Roundaville, Y.-W. Ok, K. Madani, C.-W. Chen, K. Tate, V. Upadhyaya, F. Zimbardi, 730 mV implied Voc enabled by tunnel oxide passivated contact with PECVD grown and crystallized n+ polycrystalline Si, in: 2015 IEEE 42nd Photovoltaic Specialist Conference (PVSC), IEEE, 2015, pp. 1–5.

[18] G. Nogay, J. Stuckelberger, P. Wyss, E. Rucavado, C. Allebé, T. Koida, M. Morales-Masis, M. Despeisse, F.-J. Haug, P. Löper, Interplay of annealing temperature and doping in hole selective rear contacts based on silicon-rich silicon-carbide thin films, Sol. Energy Mater. Sol. Cells 173 (2017) 18–24.

[19] A. Richter, J. Benick, F. Feldmann, A. Fell, M. Hermle, S.W. Glunz, n-Type Si solar cells with passivating electron contact: Identifying sources for efficiency limitations by wafer thickness and resistivity variation, Sol. Energy Mater. Sol. Cells 173 (2017) 96–105.

[20] J. Krügener, F. Haase, M. Rienäcker, R. Brendel, H.J. Osten, R. Peibst, Improvement of the SRH bulk lifetime upon formation of n-type POLO junctions for 25% efficient Si solar cells, Sol. Energy Mater. Sol. Cells 173 (2017) 85–91.

[21] Rolf Brendel, Robby Peibst, Contact selectivity and efficiency in crystalline silicon photovoltaics, IEEE J. Photovolt. 6 (6) (2016) 1413–1420.

[22] J.-I. Polzin, F. Feldmann, B. Steinhauser, M. Hermle, S. Glunz, Realization of TOPCon using industrial scale PECVD equipment, in: AIP Conference Proceedings, AIP Publishing LLC, 2018, p. 040018.

[23] M. Hamasaki, T. Adachi, S. Wakayama, M. Kikuchi, Crystallographic study of semi-insulating polycrystalline silicon (SIPOS) doped with oxygen atoms, J. Appl. Phys. 49 (7) (1978) 3987–3992.

[24] James Ni, Emil Arnold, Electrical conductivity of semi-insulating polycrystalline silicon and its dependence upon oxygen content, Appl. Phys. Lett. 39 (7) (1981) 554–556.

[25] J. Ruzyłło, Proceedings of the Fifth International Symposium on Cleaning Technology in Semiconductor Device Manufacturing, The Electrochemical Society, 1998.

[26] S. Kim, J. Park, P.D. Phong, C. Shin, S. Iftiquar, J. Yi, Improving the efficiency of rear emitter silicon solar cell using an optimized n-type silicon oxide front surface field layer, Sci. Rep. 8 (2018) 10657.

[27] P. Padhamnath, A. Khanna, N. Nandakumar, N. Nampalli, V. Shanmugam, A. G. Aberle, S. Duttagupta, Development of thin polysilicon layers for application in monoPoly™ cells with screen-printed and fired metallization, Sol. Energy Mater. Sol. Cells 207 (2020) 110358.

[28] M.-A.N. Eyoum, Modularly integrated MEMS technology, in, California Univ Berkeley Dept of Electrical Engineering and Computer Science, 2006.

[29] C. Park, N. Balaji, S. Ahn, J. Park, E.-C. Cho, J. Yi, Effects of tunneling oxide defect density and inter-diffused carrier concentration on carrier selective contact solar cell performance: illumination and temperature effects, Sol. Energy 211 (2020) 62–73.

[30] J. Stuckelberger, G. Nogay, P. Wyss, Q. Jeangros, C. Allebé, F. Debrot, X. Niquille, M. Ledinsky, A. Fejfar, M. Despeisse, Passivating electron contact based on highly crystalline nanostructured silicon oxide layers for silicon solar cells, Sol. Energy Mater. Sol. Cells 158 (2016) 2–10.

[31] F. Feldmann, B. Steinhauser, T. Pernau, H. Nagel, T. Fellmeth, S. Mack, D. Ourinson, E. Lohmüller, J. Polzin, A. Moldovan, Industrial TOPCon solar cells realized by a PECVD tube process, in: Presented at the 37th European PV Solar Energy Conference and Exhibition, 2020, p. 11.

[32] D. Yan, A. Cuevas, J. Bullock, Y. Wan, C. Samundsett, Phosphorus-diffused polysilicon contacts for solar cells, Sol. Energy Mater. Sol. Cells 142 (2015) 75–82.

[33] Andrea Ingenito, Gizem Nogay, Josua Stuckelberger, Philippe Wyss, Luca Gnocchi, Christophe Allebe, Jorg Horzel, Matthieu Despeisse, Franz-Josef Haug, Philipp Loper, Christophe Ballif, Phosphorous-doped silicon carbide as front-side full-area passivating contact for double-side contacted c-Si solar cells, IEEE J. Photovolt. 9 (2) (2019) 346–354.

[34] Z. Rui, Y. Zeng, X. Guo, Q. Yang, Z. Wang, C. Shou, W. Ding, J. Yang, X. Zhang, Q. Wang, H. Jin, On the passivation mechanism of poly-silicon and thin silicon oxide on crystal silicon wafers, Sol. Energy 194 (2019) 18–26.